

## Blistering Failure of Elastic Coatings with Applications to Corrosion Resistance

Surya Effendy<sup>a</sup>, Tingtao Zhou<sup>b</sup>, Henry Eichman<sup>c</sup>, Michael Petr<sup>d</sup>, and Martin  
Z. Bazant<sup>a,e,1</sup>

<sup>a</sup>*Department of Chemical Engineering, Massachusetts Institute of Technology, 77  
Massachusetts Avenue, Cambridge, MA 02138, USA*

<sup>b</sup>*Division of Engineering and Applied Sciences, California Institute of Technology, 1200 E.  
California Blvd., Pasadena, CA91125, USA*

<sup>c</sup>*Dow Coating Materials, 400 Arcola Road, Collegeville, PA19426, USA*

<sup>d</sup>*Dow Wire and Cable, 400 Arcola Road, Collegeville, PA19426, USA*

<sup>e</sup>*Department of Mathematics, Massachusetts Institute of Technology, 77 Massachusetts  
Avenue, Cambridge, MA 02138, USA*

### 1. Supporting Information

#### 1.1. Table of Nondimensionalized Equations

The nondimensional equations used in the present work is summarized in table 1.

#### 1.2. Data Records

The data sets corresponding to figure 8(d) and figure 5(a) of the main text are recorded for posterity in table 2 and table 3, respectively.

---

<sup>1</sup>Corresponding author: bazant@mit.edu

Equation	Note
$\bar{A} = \pi \bar{r}^2 \frac{2(1-\cos \psi)}{\sin^2 \psi}$	Stretched area
$\bar{V} = \frac{\pi \bar{r}^3}{3} \frac{\cos \psi (\cos^2 \psi - 3) + 2}{\sin^3 \psi}$	Blister volume
$\bar{\Pi} = \frac{2\bar{\gamma} \sin \psi}{\bar{r}}$	See equation 6
$\bar{\gamma} = \frac{\bar{E}}{6(1+K_{\text{MR}})} \left[ 1 - \left( \frac{\sin^2 \psi}{2[1-\cos \psi]} \right)^3 \right] \left[ 1 + K_{\text{MR}} \frac{2(1-\cos \psi)}{\sin^2 \psi} \right]$	See equation 7
$\frac{2(1-\cos \psi)}{\sin^2 \psi} \leq 1 + \epsilon$	See equation 8
$\frac{d\bar{r}}{dt} = \bar{k}_{\text{ad}} (\bar{\sigma}_{\text{ad}} - \bar{\sigma}_{\text{ad}}^*) H(\bar{\sigma}_{\text{ad}} - \bar{\sigma}_{\text{ad}}^*)$	See equation 9
$\bar{\sigma}_{\text{ad}} = \bar{\gamma} \frac{2(1-\cos \psi)}{\sin^2 \psi}$	See equation 10
$\bar{\Pi} = \sum_i \frac{\bar{n}_i}{\bar{V}} - \bar{C}_{i,\text{out}}$	See equation 11
$\frac{d\bar{n}_i}{dt} = \bar{J}_i \bar{A} + \nu_i \bar{R}_s \bar{A}_{\text{base}} + \eta_i \bar{R}_p \bar{V}$	See equation 12
$\bar{J}_i = \delta_i (\bar{C}_{i,\text{out}} - \bar{C}_i) \frac{2(1-\cos \psi)}{\sin^2 \psi}$	See equation 13
$\bar{R}_s = -\frac{\delta_{\text{O}_2}}{\nu_{\text{O}_2}} (\bar{C}_{\text{O}_2,\text{out}} - \bar{C}_{\text{O}_2}) \left[ \frac{2(1-\cos \psi)}{\sin^2 \psi} \right]^2$	See equation 14
$\bar{R}_p = \bar{k}_p (-\eta_{\text{Fe}^{2+}} \ln \bar{C}_{\text{Fe}^{2+}} - \eta_{\text{OH}^-} \ln \bar{C}_{\text{OH}^-} - \bar{\mu}^\ominus)$	See equation 16
$\bar{\mu}^\ominus = \ln \left[ \left( -\frac{z_{\text{OH}^-}}{z_{\text{Fe}^{2+}}} \right)^{\eta_{\text{OH}^-}} \frac{1 + \bar{K}_{\text{FeCl}^+} \bar{C}_{\text{Cl}^-}}{1 + \bar{K}_{\text{FeCl}^+} \bar{C}_{\text{Cl}^-,\text{out}}} \right]$	See equation 17
$- \left( \frac{\bar{\beta}_p}{\bar{C}_{\text{Fe}(\text{OH})_2}} \right)^2$	

Table 1: Complete set of nondimensionalized equations used in the present work. Note that the conventional  $s_1$  and  $s_{-1}$  parameters used to describe Mooney-Rivlin solids (see equation 7) has been replaced with an equivalent pair of parameters: nondimensional Young's modulus  $\bar{E}$  and stress equilibrium constant  $K_{\text{MR}}$ .

### 1.3. Table of Experiments

The list of experiments performed to validate the critical delamination length hypothesis is shown in table 4. The result for experiment 9 has been shown in figure 9 of the main text; in figure 1, we summarize other findings of interest.

The top row of figure 1 shows the replicate run of figure 9 of the main text, with similar qualitative results albeit with earlier rust spot nucleation and faster blister growth. In particular, we still observe dark-green coloration at the edge of the blister at all points in time and the eventual development

1.89 $\mu\text{g}$		6.40 $\mu\text{g}$		8.50 $\mu\text{g}$	
t [days]	Vol. [nL]	t [days]	Vol. [nL]	t [days]	Vol. [nL]
7.8	8.3	6.0	22.8	3.5	30.5
29.2	17.0	16.1	42.3	30.4	86.5
65.7	29.7	23.7	61.2	56.4	109.0
78.6	22.4	73.7	97.2	77.5	130.6
95.4	32.1	98.0	107.4	107.1	154.3
115.7	28.0	103.9	122.8	142.0	171.2
134.7	28.4	122.6	127.0	149.2	186.2
149.3	31.1	156.6	144.3		

Table 2: Blister volume data for the undercoat salt immersion experiment described in [25]. Note that this data set is extracted from a figure published therein.

Water mole fraction $x_{\text{H}_2\text{O}}$	Water diffusivity in polyurethane $D_{\text{H}_2\text{O}}$ [ $\mu\text{m}^2/\text{hr}$ ]
0.65	37.5
0.85	70.5
0.90	89.9
0.93	108.1

Table 3: Diffusion data for the steady-state Payne cup measurement described in [25]. Note that this data set is extracted from a figure published therein.

Number	Pigmented?	Teflon?	Diameter [mm]	Pinhole defect?
1	Yes	Yes	$\sim 5$	Yes
2	Yes	Yes	$\sim 5$	No
3	Yes	Yes	$\sim 15$	Yes
4	Yes	Yes	$\sim 15$	No
5	Yes	No	-	Yes
6	Yes	No	-	No
7	No	Yes	$\sim 5$	Yes
8	No	Yes	$\sim 5$	No
9	No	Yes	$\sim 15$	Yes
10	No	Yes	$\sim 15$	No
11	No	No	-	Yes
12	No	No	-	No

Table 4: List of critical delamination length experiments. Each experiment is repeated twice.

of pocket-shaped patterns. Differences in observation can be explained by the manual introduction of pinhole defects, which is difficult to control; otherwise, the observations made in section 4 of the main text are replicable.

The middle row of figure 1 shows the result of experiment 10, which is identical to experiment 9, except no pinhole defect is added. This delays rust spot nucleation, which first appears at 144 hours, although the growth of the blister proceeds at a typical speed once nucleation has begun. Once again, a dark-green patina is observed at the edge of the blister at all points in time. We note that the nucleation event occurs at the edge of the Teflon patch (dotted red line) and grows more slowly along the Teflon patch, suggesting that the Teflon patch imparts some degree of corrosion resistance. This justifies our hesitation in claiming that the result in figure 9 of the main text supports the scaling relation  $r \sim \exp t$ .

The replicate run for the middle row of figure 1 does not show any undercoat rust, except the one occurring at the edge of the measurement area. More generally, all experiments on non-pigmented coatings with no pinhole defect do not develop undercoat rust, with the exception of the result presented in the middle row of figure 1. This confirms the hypothesis made by Funke that the addition of a pinhole defect can initiate osmotic blistering [23].

The bottom row of figure 1 shows the result for experiment 4, which is identical to experiment 10 except for the use of  $\text{TiO}_2$  pigment particles. The frequency of blister formation is greatly increased relative to non-pigmented coatings. We originally suspected that  $\text{TiO}_2$  particles either participate in or encourage the formation of pinhole defects around which blisters grow; however, this hypothesis conflicts with the observation that no unstable growth occurs, unlike that seen in the top and middle rows of figure 1. The lack of growth suggests that these blisters occur due to entrapped soluble components, implying that the presence of  $\text{TiO}_2$  encourages the formation of pockets of soluble components. The exact mechanism is not clear; we speculate on adsorption of ions on the charged surface of  $\text{TiO}_2$ .

The second and third images of the bottom row of figure 1 are identical except for a dotted red line showing the location of the underlying Teflon patch. Comparing these two images, we observe that the edge of the Teflon patch exhibits a greatly increased frequency of blister formation. It is not clear why this should be the case; we speculate on the entrapment of soluble components at the edge of the Teflon patch, which could also explain the location of the nucleation event in the middle row of figure 1. The same observations are also made for the replicate run of experiment 4.

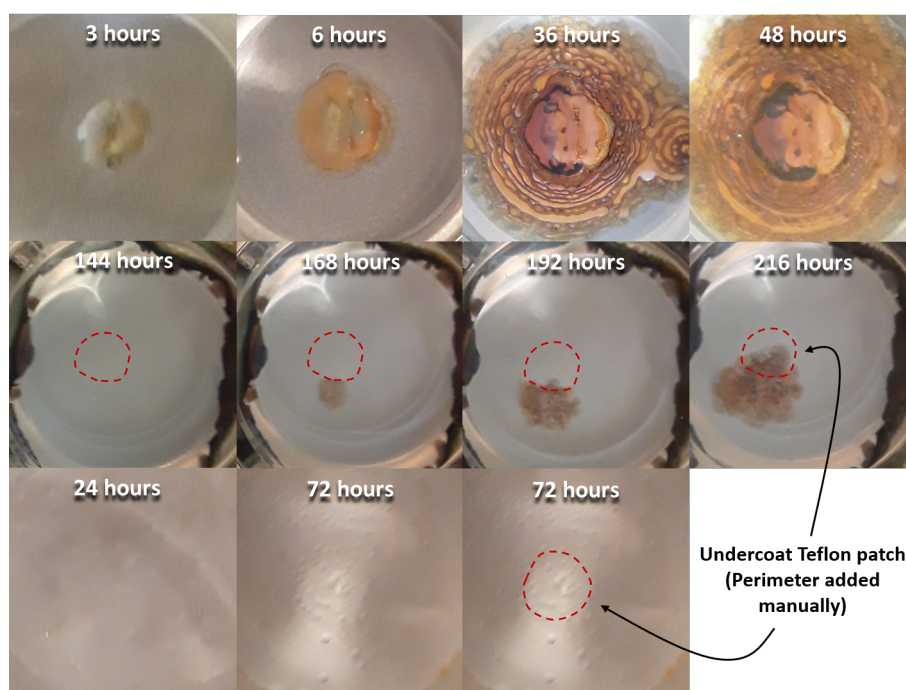


Figure 1: Top row: replicate result for experiment 9. Middle row: experiment 10. Bottom row: experiment 4.